Excitation of zonal flows and their impact on dynamics of edge pedestal collapse

Hogun Jhang[1], Helen H. Kaang[1], S. S. Kim[1], T. S. Hahm[1,2], R. Singh[1] and T. Rhee[1]

[1]National Fusion Research Institute, 52, Yeoeun-dong, Yusung-Gu, Daejon, Rep. of Korea
[2]Department of Nuclear Engineering, Seoul National University, Seoul, Rep. of Korea

Corresponding Author: hgjhang@nfri.re.kr

Abstract:

We study the role of zonal flows in edge pedestal collapse using a reduced magnetohydrodynamic (MHD) model. A dramatic change of dynamics happens when ideal ballooning modes are stabilized. A detailed analysis shows that a zonal flow driven instability is developed due to a strong excitation of zonal vorticity, resulting in secondary crashes. The presence of subsidiary bursts after a main crash increases the effective crash time and energy loss. These simulation results resemble the behavior of compound edge localized modes (ELMs). Thus, our results indicate that a complete understanding of ELM crash dynamics requires the self-consistent inclusion of nonlinear zonal flows-MHD interaction and transport physics.

1 Introduction

Understanding dynamical processes involved in the edge localized mode (ELM) crash and the subsequent energy loss has been one of the central issues in fusion plasma research for decades. A popular idea regarding the onset of ELMs is based on a linear picture: ELMs are generated by the destabilization of ideal peeling-ballooning modes[1]. In contrast to this linear picture, recent nonlinear MHD simulations emphasize the role of nonlinear dynamics in ELM crashes[2, 3, 4, **?**]. In particular, Rhee et. al. highlight the nonlinear processes leading to magnetic field line stochastzation in the pedestal collapse[**?**]. They showed that various nonlinear energy exchange mechanisms are involved in crash dynamics.

An important missing piece in previous nonlinear simulations is the absence of zonal flows (ZFs). The main purpose of this paper is to investigate the possible role of ZF during a pedestal collapse. For instance, one may expect that ZFs and the secondary tearing parity modes (STM) might share the free energy released from ballooning modes (BMs) in the early stage of collapse. This may potentially extend the collapse time due to the delay of the stochastization process. To study the impact of ZFs on pedestal collapse, we perform simulations of edge pedestal collapse using a three-field reduced MHD model implemented in the BOUT++ framework[6].

2 Simulation Model

We carry out a computational study based on a reduced MHD model consisting of vorticity and pressure evolution equations, and the Ohms law,

$$m_i n \frac{\partial U}{\partial t} = -m_i n \mathbf{V}_E \cdot \nabla U + B_0^2 \nabla_{||} \left(\frac{J_{||}}{B_0} \right) + 2\mathbf{b}_0 \times \kappa_0 \cdot \nabla P, \quad (1)$$

$$\frac{\partial P}{\partial t} = -\mathbf{V}_E \cdot \nabla P - \frac{10}{3} \frac{P_0}{1 + 5\beta/6} \frac{\mathbf{b}_0 \times \kappa_0 \cdot \nabla \Phi}{B_0} + f_K v_e^2 D_{RR} \frac{\partial^2 P_0}{\partial r^2}, \quad (2)$$

$$\frac{\partial A_{||}}{\partial t} = -\nabla_{||} \Phi + \frac{\eta}{\mu_0} \nabla_\perp^2 A_{||} - \frac{\eta_H}{\mu_0} \nabla_\perp^4 A_{||}, \quad (3)$$

where variables with subscripts 0 and 1 denote equilibrium and perturbed quantities, respectively, while those without subscripts mean total quantities. $\mathbf{V}_E = \mathbf{b}_0 \times \nabla \Phi / B_0$, $U = (1/B_0)\left(\nabla_\perp^2 \Phi + (1/en)\nabla_\perp^2 P\right)$ is the vorticity. $\kappa_0 = \mathbf{b}_0 \cdot \nabla \mathbf{b}_0$, $\beta = 2\mu_0 P_0 / B_0^2$, and $J_{||} = J_{||0} - \nabla_\perp^2 A_{||}/\mu_0$ is the parallel current including both equilibrium and perturbation parts. η (η_H) is the resistivity (hyper-resistivity) which is related to the Lundquist number (hyper-Lundquist number) $S = \mu_0 R_0 V_A / \eta = 10^9$ ($S_H = \mu_0 R_0^3 V_A / \eta_H = 10^{12}$) with the major radius $R_0 = 3.5$ (m) and the Alfven speed $V_A = 9.5 \times 10^6$ msec^{-1}.

The second term of the right hand side (RHS) of Eq. (2) stems from the divergence of the $E \times B$ velocity. This term has not been kept in the previous work [5]. Alongside the last term in RHS of Eq. (1), it describes a generation of geodesic acoustic modes (GAMs) through a coupling of Φ_{00} and P_{10}. The third term of the RHS of Eq. (2) represents a parallel heat loss through stochastic magnetic fields in accordance with the revised Rechester-Rosenbluth model[7].

The main difference between the present model and the previous ones is that we keep the zonal component of vorticity (U_{00}) in Eq. (1) and the perpendicular compressibility in Eq. (2) whose forms are given explicitly,

$$\frac{\partial U_{00}}{\partial t} = -\left[\tilde{\Phi}_{mn}, \tilde{U}_{mn}\right] + \left[\tilde{A}_{||mn}, \tilde{J}_{||mn}\right] + 2\left\langle \mathbf{b}_0 \times \kappa_0 \cdot \nabla P_{10} \right\rangle, \quad (4)$$

$$\frac{\partial P_{10}}{\partial t} = -\left[\tilde{\Phi}_{m\pm1n}, \tilde{P}_{mn}\right] + \frac{10}{3} \frac{P_0}{1 + 5\beta/6} \frac{\mathbf{b}_0 \times \kappa_0 \cdot \nabla \Phi_{00}}{B_0}, \quad (5)$$

where the (m, n) component of potential, vorticity, parallel vector potential, and pressure fluctuations is denoted by $\tilde{\phi}_{mn}$, $\tilde{U}_{mn}$, $\tilde{A}_{||mn}$ and $\tilde{P}_{mn}$, respectively, $[A, B]$ is the Poisson bracket operation, and $\langle A \rangle$ represents the flux surface average of a physical quantity A. The third term represents the contribution to U_{00} from geodesic curvature coupling due to the compressibility of the $E \times B$ drift velocity . The last terms of the RHS of Eqs. (4) and (5) signify the coupling of U_{00} with the P_{10} perturbation due to geodesic curvature[8]. We refer to these terms as geodesic curvature coupling (GCC) terms. They drive GAM oscillations, making the zonal vorticity oscillatory.

The maximum normalized pressure profile, defined as $\alpha = -2\mu_0 q^2 R_0 (dP_0/dr)/B^2 = 3.87$, while the critical value of α beyond which the ideal ballooning mode is unstable, $\alpha_c = 2.75$. So, the initial pressure profile is strongly unstable to BMs. The toroidal mode number of the most unstable mode is $n = 20$.

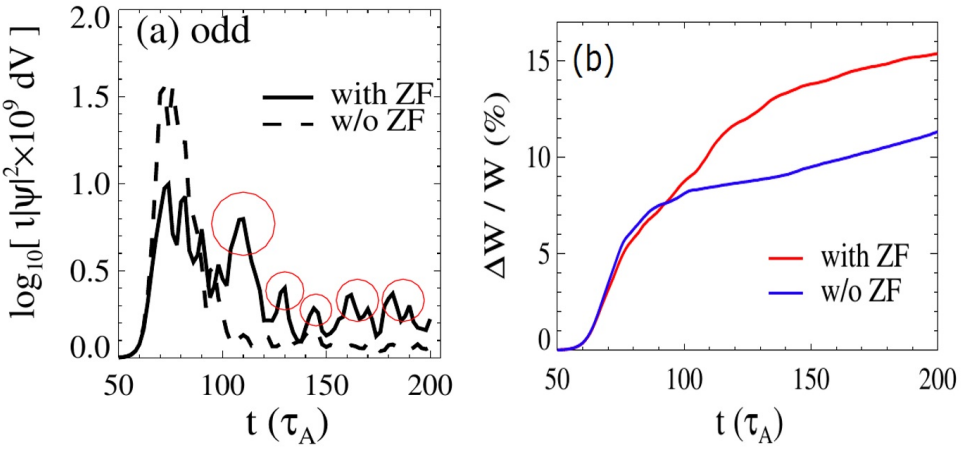

FIG. 1: Time evolution of (a) volume integrated intensities for odd parity modes and (b) the cumulative ratio of thermal energy loss to the initial thermal energy ($\Delta W/W$) during simulations. Solid (dashed) lines in (a) represent the case with (without) the inclusion of zonal flow dynamics in the simulation model.

3 Simulation Results

Previous simulation studies demonstrated the generation of strong stochastic magnetic fields as a feature of a pedestal collapse. The strong stochastization also arises in our simulations, implying the irrelevance of ZFs to the stochastization process. When ZF is present, however, the stochastization region becomes broader up to 37%, showing a restart of the stochastization front after ideal BMs are stabilized. Restart of stochastization front is particularly interesting because it may imply the possibility of a new dyanmical process other than destabilization of ideal BMs (ideal BMs are found to be stable at this time point).

A remarkable difference between the two cases can be observed if one compares time evolution of even and odd parity fluctuations. Figure 1(a) shows the volume integrated fluctuation amplitudes for even parity modes during simulations. Solid (dashed) lines represent when ZF is present (absent). One can make following observations when ZF dynamics is included in the simulation:

- The maximum amplitude of odd parity modes reduces significantly. Since the odd parity modes represent the unstable ballooning modes, it means the reduction of the initial strength of a main crash.
- After a main crash, several smaller, secondary crashes follow [marked by circles in Fig. 1(a)] in a later stage of the pedestal collapse.
- Occurrence of secondary crashes effectively prolongs the crash time and enhances the energy loss, as shown in Fig. 1(b). The energy loss enhances up to $\sim 36\%$ when ZF is included in the analysis.

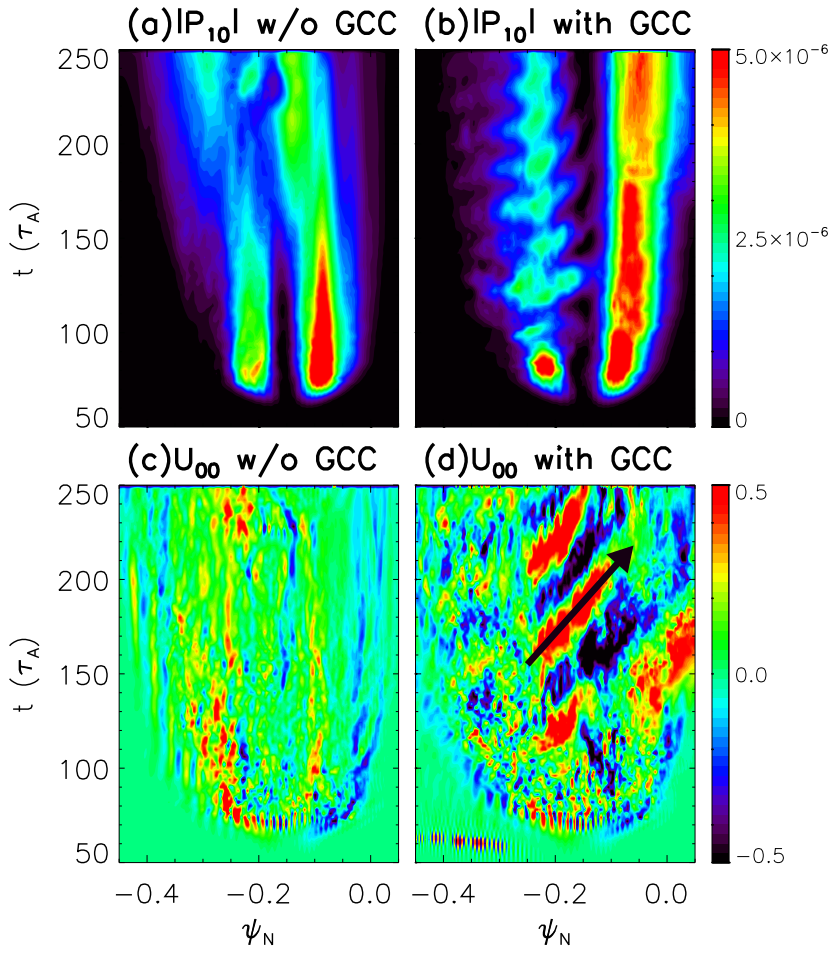

FIG. 2: Spatio-temporal evolution of $|P_{10}|$ and zonal vorticity (U_{00}) without [(a) and (c)] and with [(b) and (d)] GCC terms in Eqs. (4) and (5).

An interesting question is then the origin of the secondry crashes in the later stage of the pedestal collapse. Repeating the simulations excluding the GCC terms in Eqs. (4) and (5) showed that subsidiary crashes at later times disappear and the evolution of a crash is almost identical to the case without ZF. This suggests that GCC is likely responsible for secondary crashes after a main crash.

To make a further analysis of the GCC effect, we study the spatio-temporal evolution of the absolute value of P_{10} ($|P_{10}|$). Figures 2(a) and (b) show calculation results with (a) and without (b) the GCC terms. When $t \lesssim 100$, $|P_{10}|$ increases in both cases as a result of a strong nonlinear interaction between adjacent unstable ballooning modes, i.e., due to the first term on RHS of Eq. (5). The strong excitation occurs at two radial positions. When ZF is absent, $|P_{10}|$ diminishes at both locations after the main burst (i.e., when $t \gtrsim 100$). If we take into account the GCC terms in the model, however, $|P_{10}|$ is persistent during an entire simulation period, in particular, at outer leg position. $|P_{10}|$ at the inner

leg position shows an oscillatory behaviour in time. Interestingly, the secondary crashes are concomitant with the bursts of $|P_{10}|$ at the inner leg position shown in Fig. 2(b). This demonstrates that bursts of $|P_{10}|$ is closely related to the secondary crashes (via ZF generation through GCC) and possibly governs the zonal flow dynamics in the later stage of a pedestal collapse.

A dramatic change in zonal vorticity (U_{00}) dynamics can be seen in Figs. 2(c) and (d) where a comparison is made of U_{00} for the two cases. When the GCC terms are absent, U_{00} is governed by small scale Reynolds stress which is generated by fluctuations. The characteristic feature of this Reynolds stress generated zonal vorticity is its strongly fluctuating nature in radial direction, as can be seen at the climax of the main crash ($t \simeq 70$). When $t \gtrsim 100$, the radial wiggly structure of U_{00} disappears and no distinct feature of U_{00} is noticed (except for intermittent bursts around the saturation position), as shown in Fig. 2(c).

When GCC is taken into account [Fig. 2(d)], however, one can make the following interesting observations:

- The initial evolution of U_{00} (i.e., when $t \leq 70$) is almost identical to that of Fig. 2(c). This confirms that zonal vorticity does not play a significant role in the early phase of the pedestal collapse (or the main crash) where *ideal ballooning modes overwhelm the dynamics*.

- After the main crash, a strong zonal vorticity activity is nucleated near $\psi_N \simeq -0.23$. Note that U_{00} propagates outward in contrast to inward propagation of the stochastization front.

- The time for the second crash at $t \simeq 110$ coincides reasonably well with the time of the second burst of stochastization and radially inward propagation.

The oscillatory behaviour of U_{00} originates from the GCC terms, whose frequency can be easily estimated by taking a time derivative of Eq. (4), which yields $\omega = 2\pi f \simeq \sqrt{20/3}c_s/R$, where $c_s = \sqrt{T_e/m_i}$ and R is the major radius. Substititing the parameters being used in the simulation, $c_s \simeq 6 \times 10^5\ m/sec$ and $R \simeq 4.5\ m$, we obtain $\tau_{GCC} = 1/f \simeq 1.82 \times 10^{-5}\ sec$. This estimation accurately reproduces the oscillation period obtained from Fig. 2(d) giving rise to $\tau \simeq 50\tau_A \simeq 1.85 \times 10^{-5} sec$.

All these observations indicate that the GCC terms produce strong, oscillatory U_{00} at $\psi_N \simeq -0.23$. Reynolds and Maxwell stresses (not shown here) are almost exactly cancelled each other making their combined effects on GAM generation negligible. Once generated, it propagates outward. The propagating nature of U_{00} indeed stems from GCC. The enhancement of zonal vorticity due to GCC is in accordance with a previous study reporting the increase of ZF energy by geodesic acoustic coupling as plasma β becomes high[9]. The GCC-driven zonal flow shear plays a crucial role in the later phase of a pedestal collapse when the initially unstable BMs are significantly attenuated.

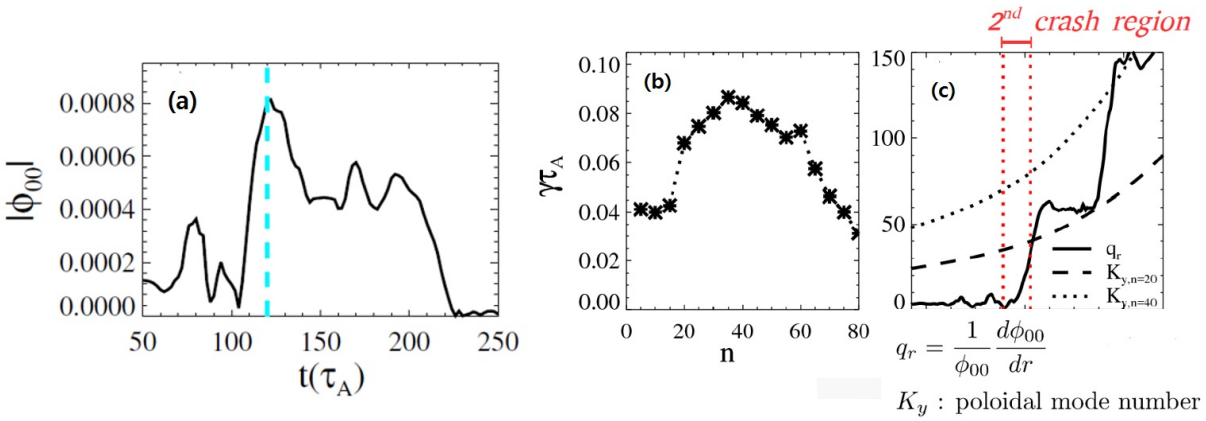

FIG. 3: Time evolution of (a) $|P_{10}|$ and $|U_{00}|$, and $|\Phi_{00}|$ at $\psi_N = -0.23$ during the simulation. Dashed line indicates $t = 120$ (just after the second crash occuring at $t = 110$) where $|\Phi_{00}|$ is maximized.

4 Interpretation and implication

The bursting nature of $|P_{10}|$ suggests destabilization of some instability. This instability, if it exists, should manifest itself after ideal MHD modes are completely stabilized because $\alpha_{max} \leq \alpha_c$ when $t \gtrsim 65\tau_A$.

To examine if a new instability other than ideal BMs is indeed present or not, we perform a linear stability analysis using the pressure profile and the radial zonal vorticity pattern at $t = 120$ corresponding to the time just after the second crash which occurs at $t \simeq 110$. Time evolution of $|\Phi_{00}|$ at $\psi_N = -0.23$ is shown in Fig. 3(a). At $t = 120$, the amplitude of $|P_{10}|$ becomes a local maximum value while that of U_{00} drops to a local minimum (not shown here). A noticeable observation is that the amplitude of zonal potential ($|\Phi_{00}|$) at $\psi_N = -0.23$ becomes maximized at this time, as shown in Fig. 3(a).

Figure 3(b) shows the results of the linear stability analysis. Surprisingly, the plasma becomes unstable at all toroidal mode numbers. In particular, higher n-modes grow faster than lower ones. Since the ideal BMs are completely stabilized at this time, one can interpret this instability as coming entirely from zonal modes.

To show that the instability is driven only when the amplitude of U_{00} is sufficiently large, we repeat the linear analysis using parameters at different time points where U_{00} is relatively weak. The linear stability analysis at $t = 70$ as a representative time point at the initial phase of the crash, shows that all modes are stable. This demonstrates that the onset of a new instability after the main crash is due to the strong excitation of zonal modes.

The fact that the mode becomes destabilized at maximum zonal potential suggests that it may be a tertiary mode or the generalized Kelvin-Helmholtz mode. This is probable if one notes that the mode begins to be destabilized at the inner region where magnetic shear is weaker than the outer region. The onset condition of ZF driven instability is that the condition $q_r \gg K_y$ should be met. Here, $q_r \equiv |(1/\Phi_{00}))(d\Phi_{00}/dr)|$ is the radial

wavenumber of zonal potential and K_y is the poloidal mode number of the mode. In order to check if this condition is met at the onset time of the instability, we calculate q_r and K_y corresponding to $n = 20$ and $n = 40$ modes, which are the two most dominant modes at this time. Figure 3(c) shows K_y and q_r as a function of ψ_N. One can see that the onset condition of the ZF-driven instability for $n = 20$ is satisfied at $\psi_N \gtrsim -0.20$ which is shifted a little from $\psi_N = -0.23$. Note that the $n = 40$ mode [dotted line in Fig. 3(c)] does not cause the tertiary instability over the entire region of the plasma in spite of its stronger destabilization than the $n = 20$ mode.

From these analyses, we conclude that the onset of ZF-driven instability is responsible for the secondary crashes after the primary one. This instability gives rise to mesoscale crashes and, consequently, increase the energy loss. It is unclear whether this instability is the tertiary mode or the generalized Kelvin-Helmholtz instability at this time, whose identification is left as a future theoretical endeavour.

Two points are worth mentioning here. First, the physics of zonal vorticity $\leftrightarrow$ GCC coupling has not been fully elucidated, even though their connection is clear in Eqs. (4) and (5). To this end, it is necessary to perform an analytic study, which is under investigation. Second, the level of GAM amplitude in this paper should be considered as a maximized one because we neglect GAM damping in our model. This, however, will not change either the dynamical processes at play, or our main conclusions, because the pedestal collapse ($\sim 100\ \tau_A$) has a shorter time scale than that of GAM damping, and so do GAM oscillations whose frequency is typically several times larger than the decay rate [10]. Thus, the inclusion of GAM damping is expected to weaken the GAM amplitude, but not expected to change our main conclusions in this paper.

The presence of secondary crashes extend the effective crash time and increase the energy loss. All these observations show symptoms of the "compound ELMs" which are routinely observed in tokamak experiments. In this sense, the present study may shed some light on the physics of compound ELMs. We note that no systematic theoretical study has been carried out on the physics origin giving rise to parasitic crashes after a main ELM crash. Clearly, these small parasitic bursts shown in experiments must not be related to the peeling-ballooning modes because they are produced when ideal modes are stable and during the relaxation phase of the pressure profile. Based on nonlinear reduced MHD simulations, we propose that parasitic crashes found in compound ELMs may originate from the excitation of strong $E \times B$ shear due to GCC and a consequent development of a mesoscale instability.

5 Summary and Conclusions

Our main findings in this study are summarized as follows: (1) A series of smaller crashes (compared to a main crash) occur due to the strong excitation of zonal flows and consequent development of a ZF-driven instability. This mesoscale instability governs the later stage of a pedestal collapse where ideal MHD modes become completely stabilized; (2) The secondary crashes increase both the effective crash time and the total energy loss.

We pointed out that they are symptoms of "compound ELMs" which are characterized

by a series of smaller crashes after a main one. These observations lead us to make a prediction that compound ELMs may be accompanied with a strong excitation of GAM perturbations.

The ZF strength observed in our work is probably an overestimation due to the absence of GAM damping in our model. There is, therefore, a caveat in direct comparison of our results to the experimental observations. Inclusion of a proper GAM damping effect is expected to make the subsidiary crashes weaker. Nevertheless, it will not change our main results and conclusions due to the smallness of the crash time compared to the typical GAM damping time. An accurate treatment of P_{10} fluctuations requires including the neoclassical Pfirch–Schuluter effect self-consistently. To do so, we need to consider parallel flow dynamics. These are left as subjects for future studies. An analytic study of ZF-driven instability in the presence of GCC is also under investigation and will be reported in the future.

Acknowledgements: This research was supported by the Research and Development Program through National Fusion Research Institute (NFRI) funded by the Ministry of Science, ICT and Future Planning of the Republic of Korea (NFRI-EN1541-2), and by the same Ministry under the ITER technology Research and Development Program (IN1504-2).

References

[1] Snyder P., Wilson H., Ferron J., Lao L., Leonard A., Osborne T., Turnbull A., Mossessian D., Murakami M. and Xu X. 2002 *Phys. Plasmas* **9** 2037

[2] Huysmans G.T.A., Pamela S., van der Plas E. and Ramet P. 2009 *Plasma Phys. Control. Fusion* **51** 124012

[3] Sugiyama L.E. and Strauss H.R. 2010 *Phys. Plasmas* **17** 062505

[4] Xi P.W., Xu X.Q. and Diamond P.H. 2014 *Phys. Rev. Lett.* **112** 085001

[5] Rhee T., Kim S.S., Jhang Hogun, Park G.Y. and Singh R. 2015 *Nucl. Fusion* **55** 032004

[6] Dudson B., Umansky M., Xu X., Snyder P. and Wilson H. 2009 *Comput. Phys. Commun.* **180** 1467

[7] Rechester A.B. and Rosenbluth M.N. 1978 *Phys. Rev. Lett.* **40** 38

[8] Miyato, M., Kishimoto, Y. and Li, Jiquan 2004 *Phys. Plasmas* **11** 5557

[9] Naulin V., Kendl A., Garcia O.E., Nielsen A.H. and Rasmussen J. Juul 2005 *Phys. Plasmas* **12** 052515

[10] Falchetto G.L., Ottaviani M., Garbet X. and Smolyakov A. 2007 *Phys. Plasmas* **14** 082304